Materials Letters 193 (2017) 283–287

Contents lists available at ScienceDirect

Materials Letters

journal homepage: www.elsevier.com/locate/mlblue

Plastic deformation of Cu single crystals containing an elliptic cylindrical void

Shuozhi Xu [a,*], Yanqing Su [b], Dengke Chen [a], Longlei Li [b]

[a] GWW School of Mechanical Engineering, Georgia Institute of Technology, Atlanta, GA 30332-0405, USA
[b] School of Earth and Atmospheric Sciences, Georgia Institute of Technology, Atlanta, GA 30332-0340, USA

ARTICLE INFO

Article history:
Received 28 December 2016
Received in revised form 21 January 2017
Accepted 2 February 2017
Available online 4 February 2017

Keywords:
Molecular dynamics
Metals
Nanovoid
Ellipticity
Dislocation

ABSTRACT

Molecular dynamics simulations are performed to study the plastic deformation of Cu single crystals containing an elliptic cylindrical void. The effects of initial void geometry including void ellipticity and void orientation angle on plastic deformation are examined by considering the stress–strain response, dislocation nucleation from the void surface, and porosity/void cross-sectional shape evolution. It is found that (i) the initial void geometry plays an important role and (ii) the growth of voids with an increasing initial ellipticity converges to that of a crack. Our results reveal the underlying mechanisms of initial void ellipticity- and orientation angle-dependent plastic deformation of metallic solids, and provide direct evidence that there is no dividing line between a void and a crack in terms of the mechanical responses of these solids.

1. Introduction

Nanovoid growth, important in ductile fracture and spallation of metals, has been the subject of extensive study for decades [1]. The following events are observed in ductile rupture of metals as plastic deformation advances: (i) voids are initiated at internal boundaries (e.g., grain boundaries) and/or due to vacancy aggregation; (ii) voids grow and change shape; (iii) large voids coalesce to form cracks which then propagate and grow; (iv) macroscopic cracks become observable and the material eventually fails [2]. The existence of voids also contributes to the hardening of metals by impeding dislocation migration [3]. As the continuum models of void growth and associated dislocation nucleation are very sensitive to the choice of various parameters and criteria (e.g., dislocation nucleation criteria and dissociation of dislocations) [4,5], atomistic methods such as molecular dynamics (MD) become the natural framework to understand the plastic response of voided metallic materials at the nano-scale [6–9].

Recently, a number of research efforts were devoted to studying the growth of elliptic cylindrical voids in Cu [10], Al [11,12], and Fe [13] by MD simulations. While these studies highlighted the significance of the initial void ellipticity in nanovoid growth, only a relatively small ellipticity ($\leqslant 0.8$) was considered. The void ellipticity is defined here as $e = \sqrt{(a^2 - c^2)/a^2}$, where a and c are length of the void major and void minor axes, respectively, as illustrated in Fig. 1 (b). Larger initial void ellipticity is worth investigating because the shape of the void would approach that of a crack as the void ellipticity approaches 1. While much MD work [14–17] has explored deformation of metals containing a crack, it remains unexplored to our best knowledge how a voided material grades into a cracked material as the initial void ellipticity increases. To address this, we conduct large scale MD simulations to quantify the effects of initial void ellipticity and orientation angle on tensile deformation of voided solids in face-centered cubic (FCC) Cu single crystals.

2. Materials and methods

The simulation cell for nanovoid growth study is presented in Fig. 1, with a model size of 15.1 nm (L_x) by 100.1 nm (L_y) by 100.1 nm (L_z) along the x, y, and z directions, respectively. Previous MD simulations [11,18] suggested that our simulation cells are large enough to ignore size effects on the onset of plasticity. The lattice orientations are $x[100]$, $y[010]$, and $z[001]$, with periodic boundary conditions applied along all directions. The lattice parameter is 3.615 Å, and each computational cell contains about 12.31 millions atoms. An elliptic cylindrical void is generated by removing all atoms throughout the specimen along the x axis and within the cross sectional shape on the y-z plane. The center of the void cross section, with an initial ellipticity of e, is at the center of the specimen. The void orientation angle θ is formed between the void major axis and the y axis. In this work, e varies from 0.8,

* Corresponding author.
E-mail address: shuozhixu@gatech.edu (S. Xu).

http://dx.doi.org/10.1016/j.matlet.2017.02.005
0167-577X/

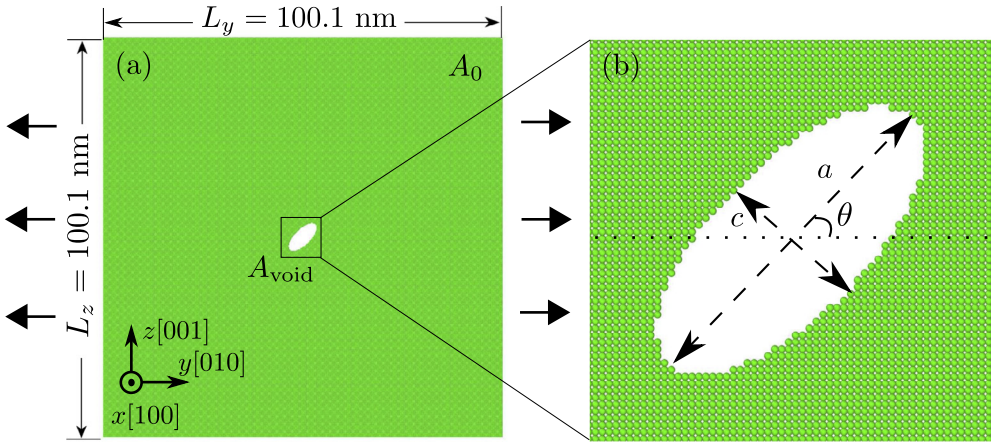

Fig. 1. Simulation cell of a Cu single crystal containing an elliptic cylindrical void formed by removing all atoms throughout the x axis and within the cross sectional shape on the y-z plane. The depth of the model in one supercell $L_x = 15.1$ nm. a and c are the length of the void major and void minor axes, respectively. The orientation angle θ, formed between the void major axis and the y axis, is either $0^\circ, 45^\circ$, or 90°. $A_0 = L_y L_z$ is the initial simulation cell area, and A_{void} is the cross-sectional area of the void; both are on the y-z plane.

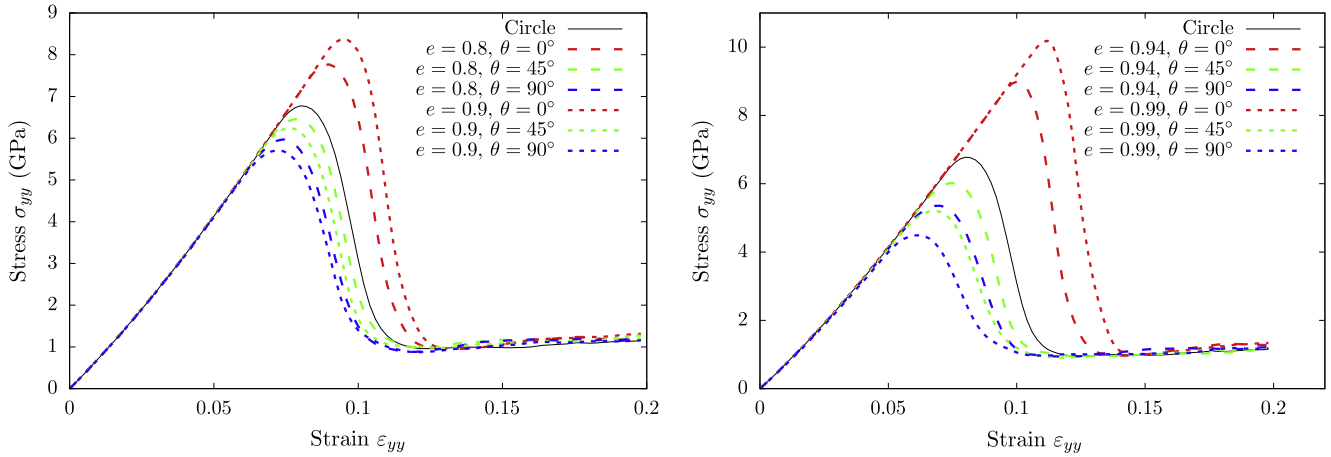

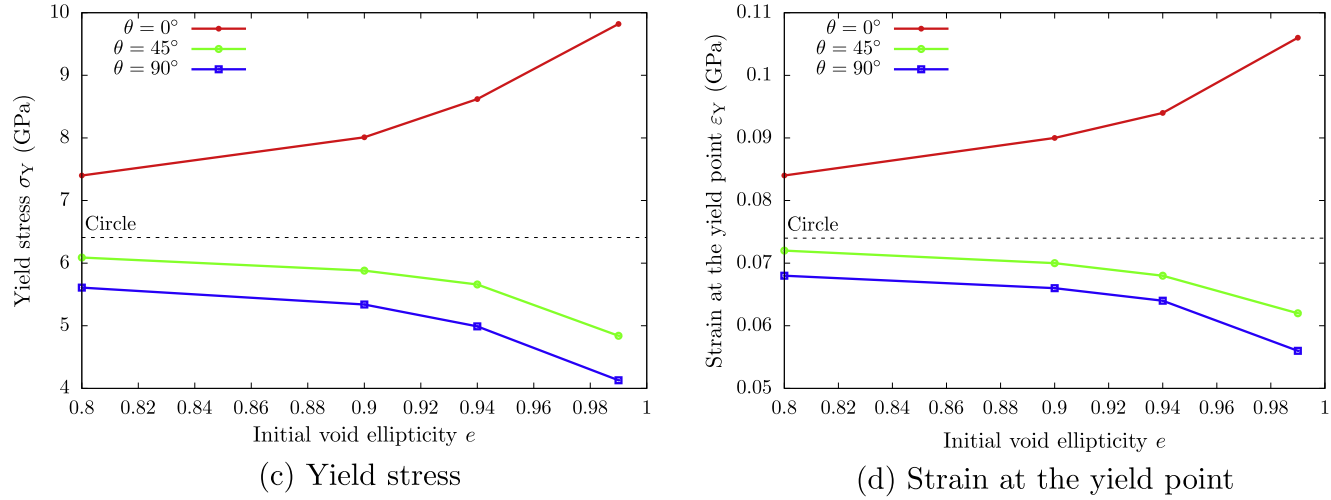

Fig. 2. Stress–strain curves in the cases of initial void ellipticity (a) $e = 0.8$ and 0.9, (b) $e = 0.94$ and 0.99, with initial void orientation angle $\theta = 0^\circ, 45^\circ$, or 90°. (c) Yield stress σ_Y and (d) strain at the yield point ε_Y as a function of both e and θ are also presented. The cases with an initially circular cylindrical void are given as solid curves in (a) and (b) and horizontal dash lines in (c) and (d) for references.

0.9, 0.94, to 0.99, while θ is either $0^\circ, 45^\circ$, or 90°. The growth of a cylindrical void with an initially circular cross section ($e = 0$), in which case varying θ takes no effect, is also studied as a reference. For all e and θ, the initial void area on the y-z plane is $\pi ac = 9\pi$ nm^2, resulting in an initial porosity $f_0 = 0.23\%$.

The embedded-atom method potential of Mishin et al. [19] is adopted for interatomic interactions in Cu. The parallel code LAMMPS [20] is employed for all atomisitc simulations. The conjugate gradient algorithm is employed to obtain the energy minimized configuration, before dynamic relaxation is conducted for 20 ps to reach an equilibrium state. Upon reaching equilibrium, a uniaxial dynamic tensile deformation is applied by changing the volume of the simulation box along the y direction at a strain rate of 10^9 s^{-1}. In all dynamic simulations, a Velocity Verlet algorithm with a time step of 2 fs is employed to update the atomic positions, and a Nosé-Hoover NPT integrator is used to maintain a constant temperature of 10 K as well as zero normal stresses along both x and z directions. Note that the effects of temperature, strain rate, loading direction, initial porosity, and time step on nanovoid growth have been quantified in our early work [10,13]. Simulation results are visualized using OVITO [21]. Some runs were completed using Comet and Bridges on Extreme Science and Engineering Discovery Environment (XSEDE) [22].

3. Results and discussion

In all cases, dislocations begin to nucleate from the void surface (denoted as the yield point) prior to the maximum stress. The normal stress along the y axis σ_{yy} with respect to the uniaxial strain along the same direction ε_{yy} is plotted in Fig. 2(a and b) for different initial void ellipticity e and orientation angle θ, with the case of

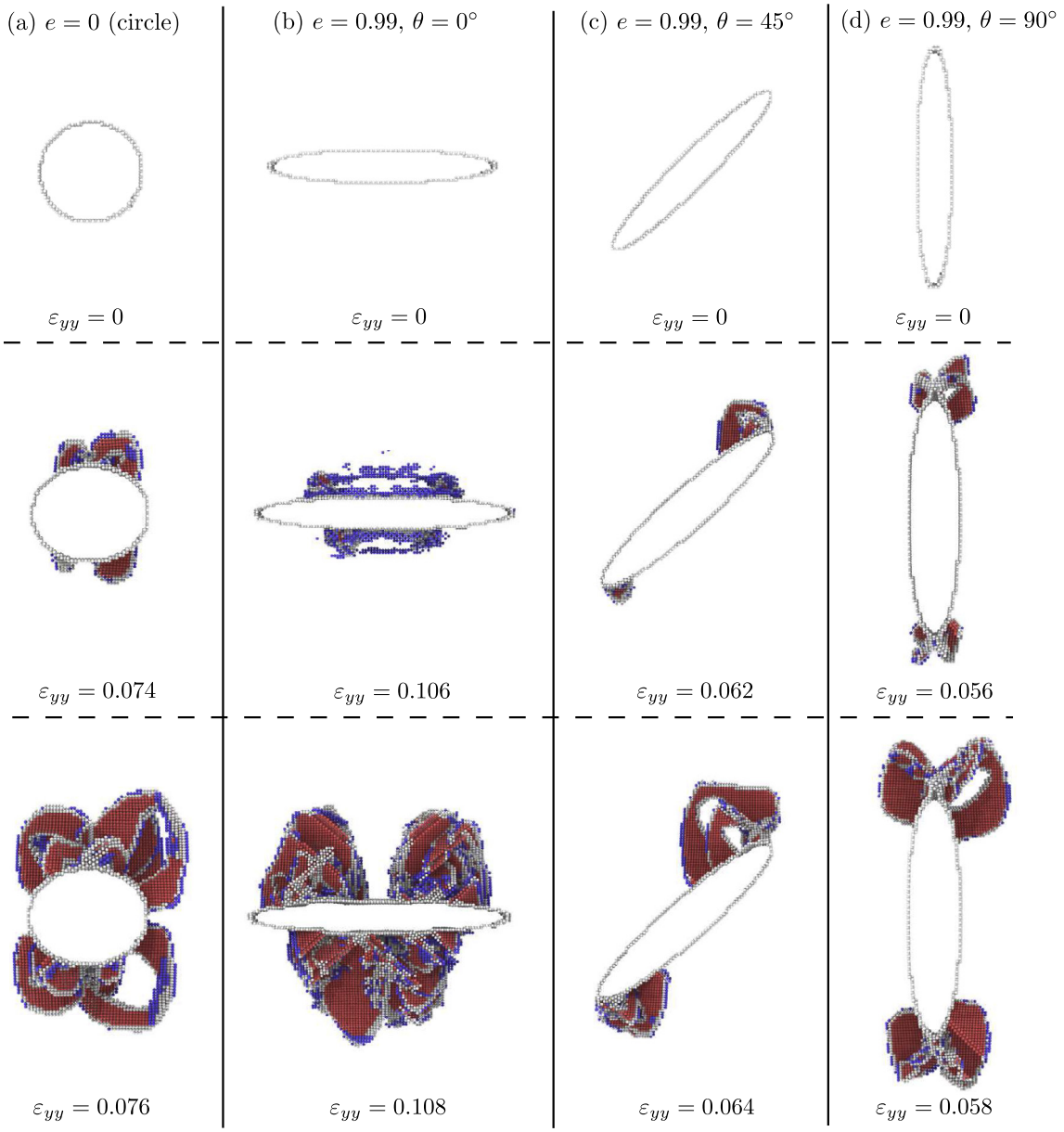

Fig. 3. Snapshots of dislocation nucleation from the surface of voids with different initial ellipticity e and orientation angle θ. Each column corresponds to the same initial void but at different uniaxial strain ε_{yy}. The second row represents the onset of plasticity, with the same critical strains as in Fig. 2(d). Atoms are colored by adaptive common neighbor analysis [23]: red are of local hexagonal close-packed structure, blue are body-centered cubic atoms, white are of unknown local structure, while all FCC atoms are removed. (For interpretation of the references to colour in this figure legend, the reader is referred to the web version of this article.)

an initially circular void presented as a reference. It is shown that (i) both the slope of the stress–strain curve prior to the yield point, i.e., the Young's modulus, and the flow stress at $\varepsilon_{yy} = 0.2$ are roughly invariant with respect to e and θ, and (ii) the influence of θ on the stress–strain response is more pronounced for a larger e, in agreement with our previous work [10,13]. The yield stress σ_Y and the corresponding strain at the yield point ε_Y are plotted as a function of e and θ in Fig. 2(c and d). Compared with an initially circular void, for the same e, all elliptic voids with $\theta = 0^\circ$ have higher σ_Y and ε_Y while those with $\theta = 45^\circ$ and 90° have lower σ_Y and ε_Y. This is because for an initially elliptic void, a larger θ results in a larger void cross-sectional area on the x-z plane, increasing the effective normal stress along the y direction, promoting dislocation nucleation, and advancing the yield point.

Fig. 3 presents snapshots of dislocation nucleation from the surface of an initially circular void (Fig. 3(a)) and of an initially elliptic void ($e = 0.99$) with $\theta = 0^\circ$ (Fig. 3(b)), 45° (Fig. 3(c)), and 90° (Fig. 3(d)), respectively. In all these cases, while all four {111} slip planes are equivalent in terms of the Schmid factor, dislocations are usually initiated on one slip plane, followed by activations of the others [10]. Because the top/bottom sites of the voids have the highest stress concentrations over the entire void outline, dislocations always begin to nucleate at these sites. As a result, (i) a larger outline curvature at the void top/bottom sites (e.g., the prolate void in Fig. 3(d)) initializes dislocation nucleation at a smaller uniaxial strain, (ii) a smaller outline curvature at the same sites (e.g., the oblate void in Fig. 3(b)) produces a higher dislocation density within the same time after the yield point because of a larger outline fraction with high stress concentrations. In other words, for an initially elliptic void, while a larger θ advances the initial dislocation nucleation, a smaller θ is accompanied by a more rapidly growing dislocation density; we found that the dislocation density at a large strain $\varepsilon_{yy} = 0.2$ is approximately the same in all cases. Note that after yielding, dislocations migrate away from the void and interact with other dislocations coming from the other side of the periodic boundaries, regardless of the initial simulation cell size. Thus, emphasis in this Letter is placed on investigating the materials responses prior to and shortly after the yield point.

Using an open-source code [24], we calculate and show in Fig. 4 that the void outline on the y-z plane and the porosity $f = A_{void}/A$ with an increasing strain, where A_{void} and A are the areas of the void and the model, respectively, on the y-z plane. We remark that the change in f is mainly contributed to the change in the void size, instead of the variation of the model size. After the yield point, the porosity starts to increase rapidly, with the void surface becoming irregular, non-smooth. Along the y direction, the void expands following the uniaxial tension applied on the model; along the z direction, however, there are two competitions controlling the void shape: (i) dislocation nucleation, which begins from the top/bottom sites of voids on certain {111} slip planes, push atoms away and enlarge the void asymmetrically, (ii) the Poisson' ratio of Cu, which is about 0.34 at the elastic stage and increases during plastic deformation [10], shrinks the specimen length as well as the void size. Among all voids, the initially elliptic void with $e = 0.99$ and $\theta = 0^\circ$, which has the most rapidly increasing dislocation density after the yield point as shown in Fig. 3(b), has the highest maximum porosity, after which the void size increases along the y axis only, while that along the z axis remains invariant.

We emphasize that when $\theta = 90^\circ$, the initial shape of the void approaches that of a crack as e increases, so should the plastic response of the specimen. Indeed, the process of dislocation nucleation and evolution from surfaces of a void with an increasing e becomes more alike that in the case of an edge crack as found in previous MD simulations in Cu using the same interatomic potential [17,15]; the void shape evolution when $e = 0.99$ is also similar to that of an edge crack presented in a previous MD work [16]. As e increases gradually, we observe no sharp changes in dislocation nucleation and cross sectional shape evolution, suggesting that there is no fixed dividing line between a void and a crack.

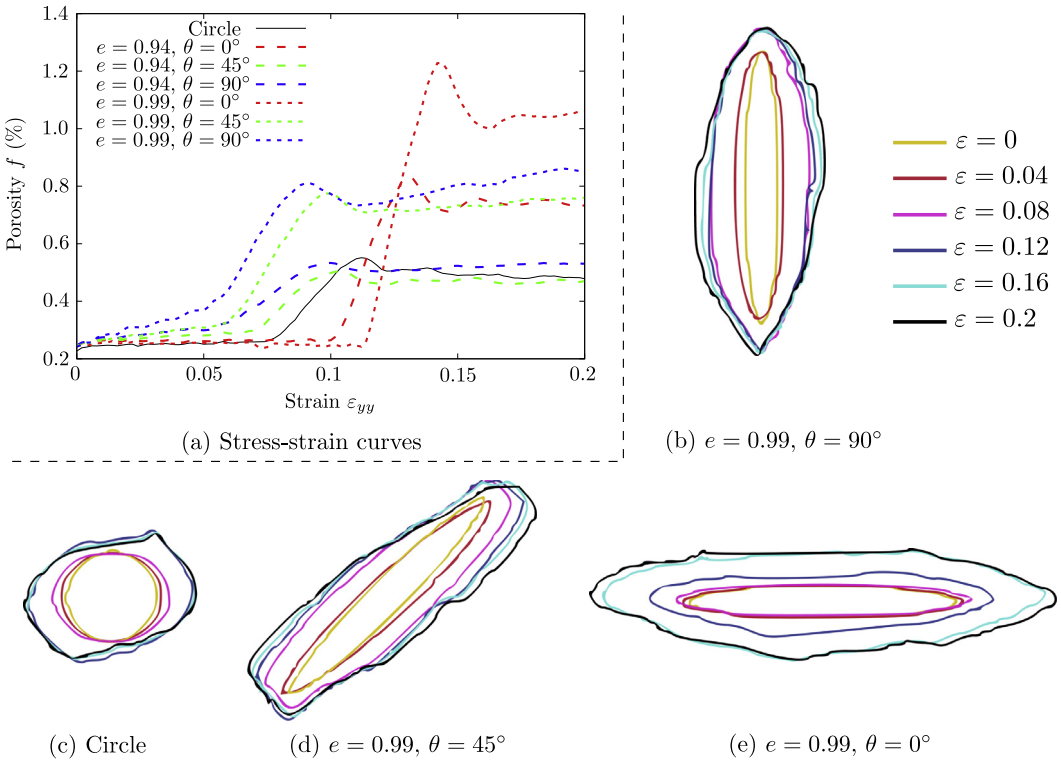

Fig. 4. (a) Porosity evolution with an increasing strain for an initially circular void and initially elliptic voids ($e = 0.94$ or 0.99), with $\theta = 0^\circ, 45^\circ$, or 90°. Also presented is the outline evolution of a void with (c) circular shape or elliptic shape with $e = 0.99$ when (b) $\theta = 90^\circ$, (d) $\theta = 45^\circ$, and (e) $\theta = 0^\circ$, respectively.

4. Conclusions

In this Letter, the effects of the initial void ellipticity and orientation angle on nanovoid growth in FCC Cu single crystals are studied using MD simulations. It is found that these two factors have substantial impacts on the stress–strain response, dislocation nucleation, and porosity/void shape evolution. Our work confirms that the growth of a void with an increasing initial ellipticity converges to that of a crack, in terms of both dislocation nucleation and void shape evolution; there is no fixed dividing line between a void and a crack. Thus, it is important to develop continuum damage models that consider voids and cracks in a unified fashion. Future work includes studying the influence of the initial void geometry in more realistic 3D simulation cells, as previous MD simulations [25] showed that 3D penny-shaped cracks lead to improved ductility compared with cracks embedded in quasi-2D models. Note that in 3D, both ellipticity and orientation will be varied in much larger, more complex datasets [26]. Additional efforts will also be devoted to explore (i) the effects of the sharpness of the crack tip and (ii) more complicated deformation such as fatigue loading [16].

Acknowledgment

We thank Mr. Thomas G. Payne for helpful discussion. This work used the Extreme Science and Engineering Discovery Environment (XSEDE), which is supported by National Science Foundation Grant No. ACI-1053575.

References

[1] M. Ponga, M. Ortiz, M.P. Ariza, Finite-temperature non-equilibrium quasi-continuum analysis of nanovoid growth in copper at low and high strain rates, Mech. Mater. 90 (2015) 253–267.
[2] X. Deng, W. Zhu, Y. Zhang, H. He, F. Jing, Configuration effect on coalescence of voids in single-crystal copper under shock loading, Comput. Mater. Sci. 50 (2010) 234–238.
[3] L. Xiong, S. Xu, D.L. McDowell, Y. Chen, Concurrent atomistic continuum simulations of dislocation- void interactions in fcc crystals, Int. J. Plast. 65 (2015) 33–42.
[4] V. Tvergaard, Void shape effects and voids starting from cracked inclusion, Int. J. Solids Struct. 48 (2011) 1101–1108.
[5] V.A. Lubarda, M.S. Schneider, D.H. Kalantar, B.A. Remington, M.A. Meyers, Void growth by dislocation emission, Acta Mater. 52 (2004) 1397–1408.
[6] T. Tang, S. Kim, M.F. Horstemeyer, Molecular dynamics simulations of void growth and coalescence in single crystal magnesium, Acta Mater. 58 (2010) 4742–4759.
[7] S.Z. Xu, Z.M. Hao, Q. Wan, A molecular dynamics study of void interaction in copper, IOP Conf. Ser.: Mater. Sci. Eng. 10 (2010) 012175.
[8] S.Z. Xu, Z.M. Hao, Y.Q. Su, Y. Yu, Q. Wan, W.J. Hu, An analysis on nanovoid growth in body-centered cubic single crystalline vanadium, Comput. Mater. Sci. 50 (2011) 2411–2421.
[9] S.Z. Xu, Z.M. Hao, Y.Q. Su, W.J. Hu, Y. Yu, Q. Wan, Atomic collision cascades on void evolution in vanadium, Radiat. Eff. Defects Solids 167 (2012) 12–25.
[10] Y. Su, S. Xu, On the role of initial void geometry in plastic deformation of metallic thin films: a molecular dynamics study, Mater. Sci. Eng.: A 678 (2016) 153–164.
[11] Y. Cui, Z. Chen, Molecular dynamics modeling on the role of initial void geometry in a thin aluminum film under uniaxial tension, Model. Simul. Mater. Sci. Eng. 23 (2015) 085011.
[12] Y. Cui, Z. Chen, Molecular dynamics simulation of the influence of elliptical void interaction on the tensile behavior of aluminum, Comput. Mater. Sci. 108, Part A (2015) 103–113.
[13] S. Xu, Y. Su, Nanovoid growth in BCC α-Fe: influences of initial void geometry, Model. Simul. Mater. Sci. Eng. 24 (2016) 085015.
[14] M. Li, W.Y. Chu, K.W. Gao, L.J. Qiao, Molecular dynamics simulation of healing of an ellipsoid crack in copper under compressive stress, Mater. Lett. 58 (2004) 543–546.
[15] T. Zhu, J. Li, S. Yip, Atomistic study of dislocation loop emission from a crack tip, Phys. Rev. Lett. 93 (2004) 025503.
[16] G.P. Potirniche, M.F. Horstemeyer, P.M. Gullett, B. Jelinek, Atomistic modelling of fatigue crack growth and dislocation structuring in FCC crystals, Proc. R. Soc. Lond. A: Math. Phys. Eng. Sci. 462 (2006) 3707–3731.
[17] H. Zhang, Y. Fu, Y. Zheng, H. Ye, Molecular dynamics investigation of plastic deformation mechanism in bulk nanotwinned copper with embedded cracks, Phys. Lett. A 378 (2014) 736–740.
[18] G.P. Potirniche, M.F. Horstemeyer, G.J. Wagner, P.M. Gullett, A molecular dynamics study of void growth and coalescence in single crystal nickel, Int. J. Plast. 22 (2006) 257–278.
[19] Y. Mishin, M.J. Mehl, D.A. Papaconstantopoulos, A.F. Voter, J.D. Kress, Structural stability and lattice defects in copper: ab initio, tight-binding, and embedded-atom calculations, Phys. Rev. B 63 (2001) 224106.
[20] S. Plimpton, Fast parallel algorithms for short-range molecular dynamics, J. Comput. Phys. 117 (1995) 1–19.
[21] A. Stukowski, Visualization and analysis of atomistic simulation data with OVITO—the Open Visualization Tool, Model. Simul. Mater. Sci. Eng. 18 (2010) 015012.
[22] J. Towns, T. Cockerill, M. Dahan, I. Foster, K. Gaither, A. Grimshaw, V. Hazlewood, S. Lathrop, D. Lifka, G.D. Peterson, R. Roskies, J.R. Scott, N. Wilkins-Diehr, XSEDE: accelerating scientific discovery, Comput. Sci. Eng. 16 (2014) 62–74.
[23] A. Stukowski, Structure identification methods for atomistic simulations of crystalline materials, Model. Simul. Mater. Sci. Eng. 20 (2012) 045021.
[24] Y. Su, Void evolution, 2016, http://www.prism.gatech.edu/~ysu65/codes/void/voids.html.
[25] J.J. Möller, E. Bitzek, On the influence of crack front curvature on the fracture behavior of nanoscale cracks, Eng. Fract. Mech. 150 (2015) 197–208.
[26] C.H. Ersland, I.R. Vatne, C. Thaulow, Atomistic modeling of penny-shaped and through-thickness cracks in bcc iron, Model. Simul. Mater. Sci. Eng. 20 (2012) 075004.